

Figure 8.20: Noise reduction and control input for two PC subsets, 138 Hz

### Principal component significance test

The significance metric listed in the last column of Table 8.2 was evaluated in a simple test. In some sense, the results from the previous section in which only the first six PCs were controlled was a test of the significance metric, because according to the values in the table, only the first six PCs were significant. In order to discuss a more interesting application of the significance metric, we assume the goal is to implement active control with only three degrees of freedom in the controller while maximizing noise reduction performance. One choice of the three PCs to control is the first three PCs of the control system, and a second choice is the three PCs with the highest significance values, corresponding to PCs 1, 2 and 4. The performance of the PC-LMS algorithm controlling PCs 1-3 was compared with the performance controlling PCs 1,2 and 4.

Time histories of the noise reduction for the two cases are shown in Fig. 8.20(a) and the corresponding control effort is shown in Fig. 8.20(b). When the most significant PCs (1,2,4) were controlled, the primary response was reduced by 15.9 dB, while controlling the first 3 PCs produced only 12.8 dB of reduction. Thus the significance metric indicates which PCs will be most useful for reducing the primary response. There is a tradeoff when higher PCs are controlled instead of lower PCs, which is apparent in Fig. 8.20(b). Controlling the fourth PC, instead of the third PC, increased the control effort from 40 Volts<sup>2</sup> to 67 Volts<sup>2</sup>. Nonetheless, in cases where the design goal is to maximize noise reduction while minimizing the degrees of freedom of the controller, the tradeoff between simplicity and control effort may be justified.

### 8.2.3 Results: 147 Hz

The noise reduction and effort penalty tests conducted at 138 Hz were repeated at a second test frequency of 147 Hz. This test frequency was close to the natural frequency of the (2,1,0) cavity mode at 150 Hz. The locations of the control actuators had been optimized for this frequency, but the noise reduction results were only slightly better than at 138 Hz.

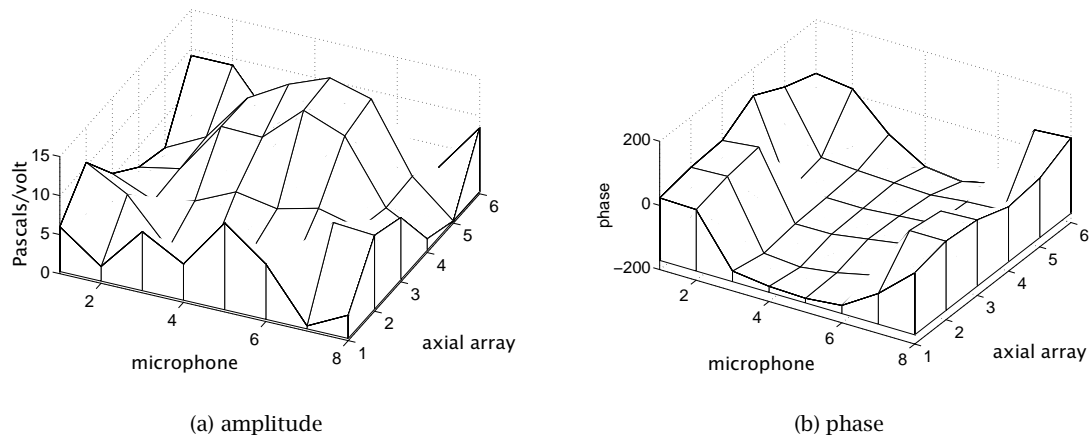


Figure 8.21: Primary response at 147 Hz

The mean square response of the microphones to background noise, measured over 60 seconds was  $0.51 \text{ Volts}^2$ . This was greater than the background noise during the 138 Hz tests, which may have been a result of conducting the tests on different days. The amplitude and phase of the primary response at 147 Hz are shown in Fig. 8.21. The shape of the response matches the shape of the  $(2, 1, 0)$  mode, with second order variation in the circumferential direction, and first order variation along the length of the shell.

Once the transfer function matrix and primary response were measured, the noise reduction was estimated as 23.2 dB, which represents only a 0.7 dB increase over the predicted reduction at 138 Hz. This indicates the actuator array performed well at either test frequency. The properties of the principal components of the control system are listed in Table 8.3. From the singular values listed in the table, the condition number is computed as  $(s_1/s_{12}) = 57.4$ . This is smaller than the condition number at 138 Hz, and perhaps as a result of the improved conditioning at 147 Hz, convergence of the filtered-x LMS algorithm was stable. The predicted noise reduction for each PC is listed in the third column of the table as a percent of the primary response. The first three PCs produced the majority of the noise reduction of the controller, as the noise reduction drops off quickly for PCs four through twelve. The predicted control effort for each PC is listed in the fourth column. Note that although the eleventh PC accounts for 47% of the total control effort, it reduces the primary by only 0.5%. The significance of the PCs are listed in the last column of the table, and using the selection metric in Eq. 8.23, PCs 7, 10, and 12 should be eliminated from the controller.

### Convergence Behavior

The performance of the filtered-x LMS algorithm with no effort penalty was compared with that of the PC-LMS algorithm controlling all twelve PCs. The maximum step size parameter at this frequency was  $\mu_{max} = 2/s_1^2 = 0.069$ , so the step size for the filtered-x LMS algorithm was set to  $(1/4)$  of this value, or 0.017. The step sizes for the PCs in the PC-LMS algorithm were set to  $(1/16)$  of the maximum step size, or 0.004. Time histories of the sum of squared microphone responses for a five minute period are shown in Fig. 8.22. The values are plotted relative to the primary response with no control, and the predicted noise reduction is shown as a dotted line at  $-23.2 \text{ dB}$ . As at 138 Hz, the PC-LMS controller

Table 8.3: Properties of principal components at 147 Hz

PC #	singular value	noise reduction (dB)	control effort (Volts <sup>2</sup> )	significance
1	5.37	21.0	6.3	9.4
2	4.64	16.1	6.5	8.2
3	3.62	58.6	38.8	15.6
4	1.86	0.4	1.1	1.3
5	1.47	1.0	3.8	2.0
6	0.80	1.0	13.0	2.0
7	0.65	0.0	0.5	0.3
8	0.42	0.6	30.1	1.6
9	0.32	0.3	26.5	1.1
10	0.24	0.0	0.7	0.1
11	0.18	0.5	126.0	1.4
12	0.09	0.0	14.2	0.2

quickly converged and reduced the primary by 23.0 dB. The filtered-x controller did much better in this test than at 138 Hz, reducing the primary by 21.1 dB after five minutes. Note that even with a higher step size, the filtered-x LMS algorithm was still slower to converge than the PC-LMS algorithm. This was probably due to the control filter weights being updated one actuator at a time in the filtered-x controller.

The corresponding total control effort for the two controllers is shown in Fig. 8.23. The filtered-x controller was still converging after five minutes, with a terminal value of 144 Volts<sup>2</sup>. The predicted total control effort for this frequency was 267.5 Volts<sup>2</sup>, and the PC-LMS controller converged to this value. It is interesting to note the large difference between the control efforts for the two controllers but the relatively small difference in noise reduction performance. Assuming the filtered-x algorithm were to converge to the same effort as the PC-LMS algorithm, its control effort would nearly double from 144 Volts<sup>2</sup> to 260 Volts<sup>2</sup>, but the noise reduction would only increase from 21.1 dB to 23.2 dB. This illustrates how large control efforts can be expended for small amounts of noise reduction.

The control efforts for each actuator computed by the control algorithms are compared to the predicted control efforts in Fig. 8.24. The PC-LMS algorithm was in excellent agreement with the predicted values, whereas the filtered-x algorithm converged to control efforts that were generally smaller than the predicted values. This discrepancy may have been a result of the slow convergence of the filtered-x algorithm caused by updating the control filter weights one actuator at a time.

The predicted PC control efforts are compared with the experimentally computed values from the PC-LMS controller in Fig. 8.25, and as with the data in Fig. 8.24, the PC inputs agree closely with the predicted values.

### Control Effort

The implementation of a control effort penalty in both controllers was compared at 147 Hz. The filtered-x LMS algorithm was tested with values of  $\beta$  of 10, 1, and 0.1. The noise reduction and control effort for the largest and smallest values of  $\beta$  are compared to the PC-LMS algorithm controlling the first two PCs, and the first five PCs, respectively. The noise reduction for these tests is shown in Fig. 8.26(a), and the associated control effort in Fig. 8.26(b). The results of these tests were nearly

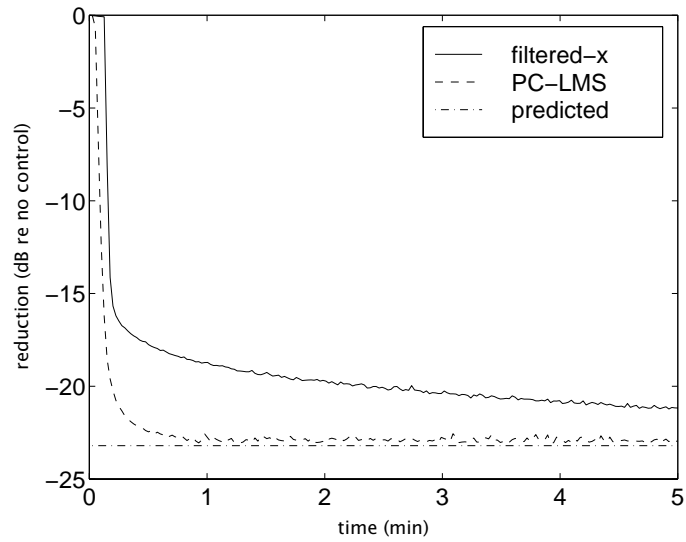


Figure 8.22: Convergence of the sum of squared microphone responses at 147 Hz

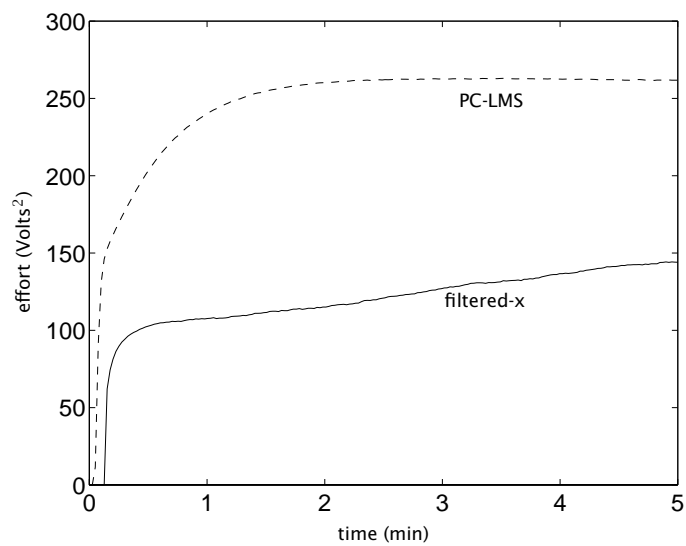


Figure 8.23: Convergence of control effort for 147 Hz

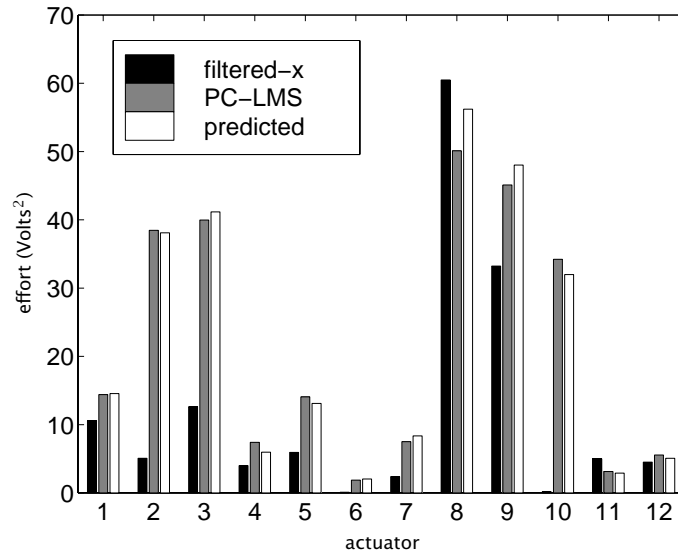


Figure 8.24: Control efforts for individual actuators at 147 Hz

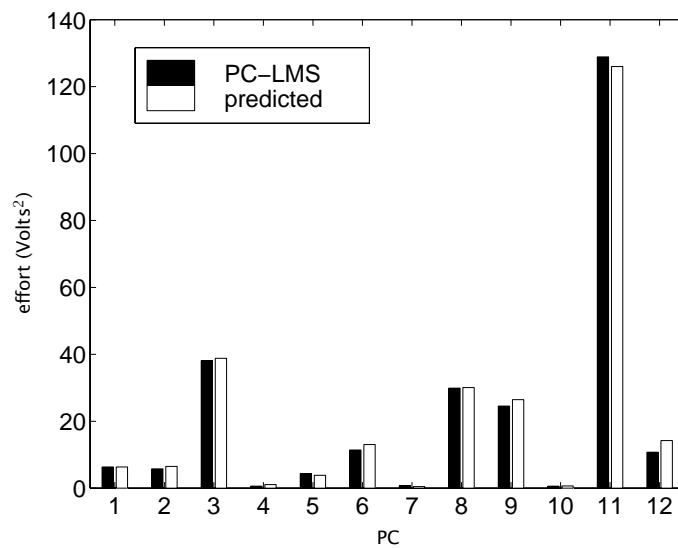


Figure 8.25: Control efforts for individual principal components at 147 Hz

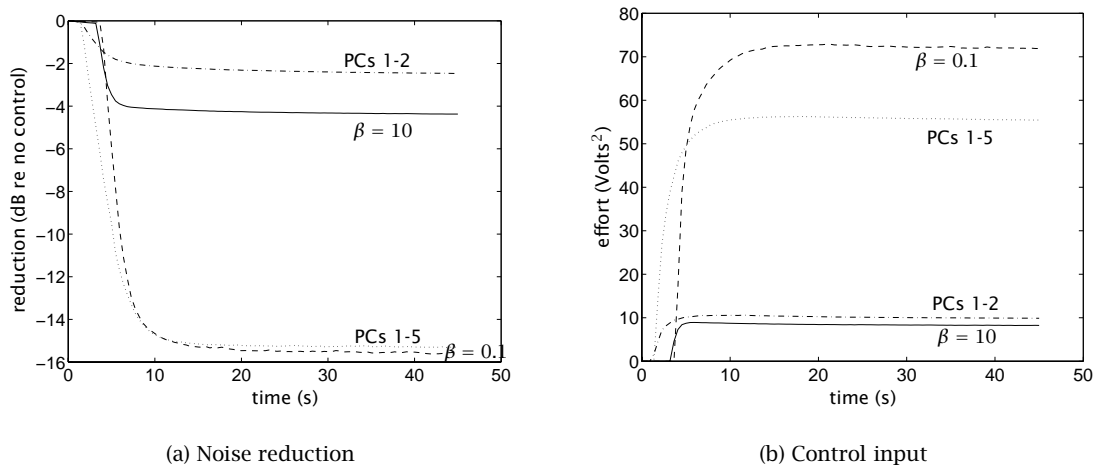


Figure 8.26: Comparison of PC-LMS and filtered-x effort penalties at 147 Hz

identical to the control effort tests at 138 Hz. For a large effort penalty ( $\beta = 10$  for filtered-x LMS, and PC-LMS controlling only the first two PCs), the filtered-x LMS controller obtained greater noise reduction with the same amount of control effort as the PC-LMS controller. However, for the small effort penalty ( $\beta = 0.1$  and PC-LMS controlling the first five PCs), the PC-LMS controller obtained nearly the same amount of noise reduction, but with less control effort, than the filtered-x LMS controller. These results illustrate the benefits of implementing a control effort penalty by not controlling the last few PCs of the controller.

### Principal component significance test

The significance metric listed in the last column of Table 8.3 was evaluated by comparing the noise reduction and control effort for three PC subsets. From the values listed in Table 8.3, the least significant PCs, in order of increasing significance, are 10, 12, 7, and 9. Three subsets of PCs were chosen based on the significance values; the first set consisted of PCs 1-7, and represents a baseline case. The second set consisted of PCs 1-6 and 8, where PC 7 was replaced by PC 8. The third set consisted of PCs 1-6, 8, and 11, because these were the eight most significant PCs.

Time histories of the noise reduction for the three subsets are shown in Fig. 8.27(a) and the corresponding control efforts are shown in Fig. 8.27(b). The noise reduction results indicate that as more significant PCs are added to the set being controlled, noise reduction performance improves. The best reduction was obtained with PCs 1-6, 8, and 11. The control efforts in Fig. 8.27(b) illustrate the cost of adding in the higher PCs, since these PCs require more control effort. The control effort increases dramatically when PC 11 is added to the subset of controlled PCs. These results indicate the versatility of the PC controller, and how the ability to control or not control individual PCs can be used to tailor the performance of the control system and make trade-offs between noise reduction and control effort.

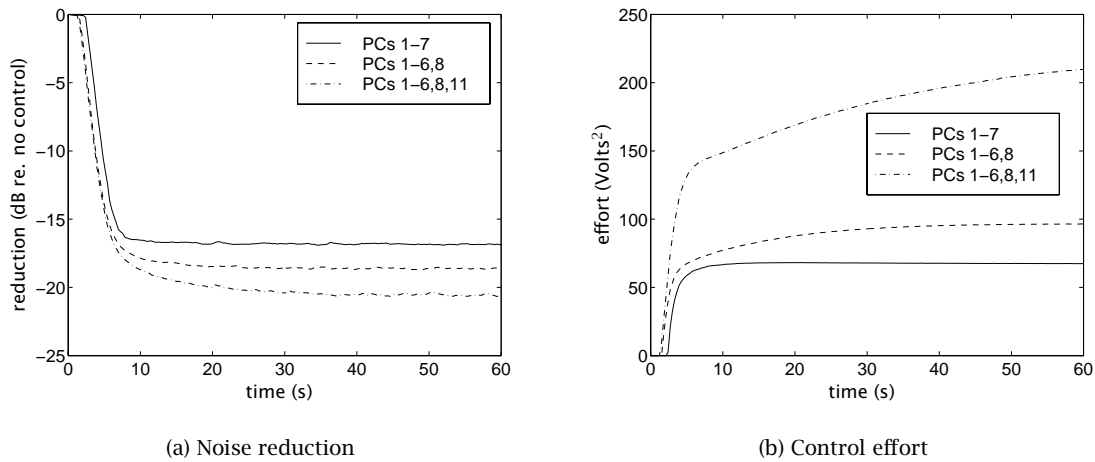


Figure 8.27: Noise reduction and control input for three PC subsets, 147 Hz

Table 8.4: Real parts of first four eigenvalues of matrix products

$\mathbf{H}_{138}^H \mathbf{H}_{138}$	$\mathbf{H}_{138}^H \mathbf{H}_{135}$	$\mathbf{H}_{138}^H \mathbf{H}_{132}$	$\mathbf{H}_{138}^H \mathbf{H}_{129}$
64.4	41.6	9.3	-16.7
19.6	10.8	11.1	10.3
5.7	7.1	6.3	3.1
3.7	2.2	1.1	0.6

## 8.2.4 Robustness to frequency variation

A simple series of tests were conducted to compare the robustness of the filtered-x LMS and PC-LMS algorithms to errors in the transfer function matrix. The errors were introduced artificially by computing the transfer function matrix at one frequency, and then using it in either control algorithm to cancel a disturbance at a different frequency. This robustness test is not a complete validation of the robustness of the PC-LMS algorithm relative to filtered-x LMS, since it is only one test and involves one kind of error that might be present in the transfer function matrix. However, it was still useful for comparing the two controllers when the transfer function matrix contained errors.

The transfer function matrix between actuators and microphones was measured at 4 frequencies: 138, 135, 132, and 129 Hz. These frequencies were chosen because they were close to 138 Hz, and a preliminary analysis suggested the adaptive control algorithms would be stable at 135 and 132 Hz, but not at 129 Hz, assuming the transfer function matrix at 138 Hz was used. The transfer function matrix measured at each test frequency will be denoted here as  $\mathbf{H}_{138}$ ,  $\mathbf{H}_{135}$ , etc. From the robustness analysis of the algorithms, in Sections 3.2.2 and 4.3, the stability of convergence depends on the eigenvalues of the product of the true transfer function matrix and the estimated transfer function matrix. We will assume that the errors introduced by changing the excitation frequency are much greater than random estimation errors in the transfer function matrices. With this assumption, the matrix product whose eigenvalues must be analyzed is given by  $(\mathbf{H}_{138}^H \mathbf{H}_f)$ , where  $f$  is one of the four test frequencies.

The real parts of the first four eigenvalues of each of the four relevant matrix products are listed in Table 8.4. The real parts of the eigenvalues not shown were all positive. The values in the table

indicate the filtered-x and PC-LMS algorithms should be stable at 135 and 132 Hz, but because the real part of the first eigenvalue of  $(\mathbf{H}_{138}^H \mathbf{H}_{129})$  is negative, the algorithms will go unstable at 129 Hz. This was confirmed in the experiment, and neither algorithm could be made stable when the transfer function matrix from 138 Hz was used to control a single frequency disturbance at 129 Hz. The results given here are thus only for 138, 135, and 132 Hz.

Because the filtered-x LMS controller had difficulty converging at 138 Hz in earlier tests, a control effort penalty was added to the algorithm. An effort penalty can stabilize the convergence of the filtered-x LMS algorithm when the transfer function matrix contains errors (Boucher et al. 1991). The penalty parameter  $\beta$  was set to 1.0, since initial tests shows that this value was sufficient to stabilize convergence of the algorithm at 138 Hz and still produce acceptable noise reduction. An effort penalty was also implemented in the PC-LMS algorithm by controlling only the first six PCs of the control system. This number was chosen as a compromise between too few and too many degrees of freedom for the PC controller. If the controller had too few degrees of freedom, it might not obtain good noise reductions at the different test frequencies, but if it had too many degrees of freedom, it might be susceptible to errors in the last few PCs at the different test frequencies that would cause convergence to be unstable.

In these tests, the transfer function matrix at 138 Hz was downloaded to the DSP, either in its entirety for the filtered-x LMS algorithm, or in terms of its singular vectors, for the PC-LMS algorithms. Results are given here for control at three frequencies: 138, 135 and 132 Hz. Both control algorithms were allowed to converge for 5 minutes, at which point the noise reduction and control efforts were saved. The noise reduction and corresponding control effort obtained by the two control algorithms are shown in Fig. 8.28. The values are plotted as a function of the test frequency. The results at 138 Hz are baseline results, since the transfer function matrix was accurate at this frequency. At 138 Hz, the filtered-x LMS controller reduced the primary by 15.6 dB, dropping to 9.3 dB at 135 Hz, and to 6.1 dB at 132 Hz. The PC-LMS algorithm reduced the primary by 20.6 dB at 138 Hz, dropping to 17.7 dB at 135 Hz, and to 14.6 dB at 132 Hz. The noise reduction of the PC-LMS algorithm did not drop as much as the filtered-x LMS algorithm as the errors in the transfer function matrix increased.

The control efforts for both controllers are shown in Fig. 8.28(b). As the test frequency changed from 138 Hz to 132 Hz, the effort for the PC-LMS controller dropped from 104.7 Volts<sup>2</sup> to 66.8 Volts<sup>2</sup>. The effort for the filtered-x LMS controller only dropped from 92.5 Volts<sup>2</sup> to 81.7 Volts<sup>2</sup>. The PC-LMS controller maintained high noise reduction levels using less control effort than the filtered-x LMS algorithm.

These results confirm that the robustness of the PC-LMS and filtered-x algorithms is equivalent, at least in the simple test conducted here. Neither controller could converge when the transfer function matrix from 138 Hz was used at 129 Hz, but both could converge at 138, 135, and 132 Hz. Although the PC-LMS controller was controlling a subset of the PCs, its performance was not affected as much as the filtered-x algorithm. The PC-LMS algorithm maintained high noise reduction levels and used less control effort than the filtered-x LMS algorithm. This demonstrates that controlling a subset of PCs is a better alternative to dealing with modeling errors than using a uniform effort penalty in the filtered-x LMS algorithm.

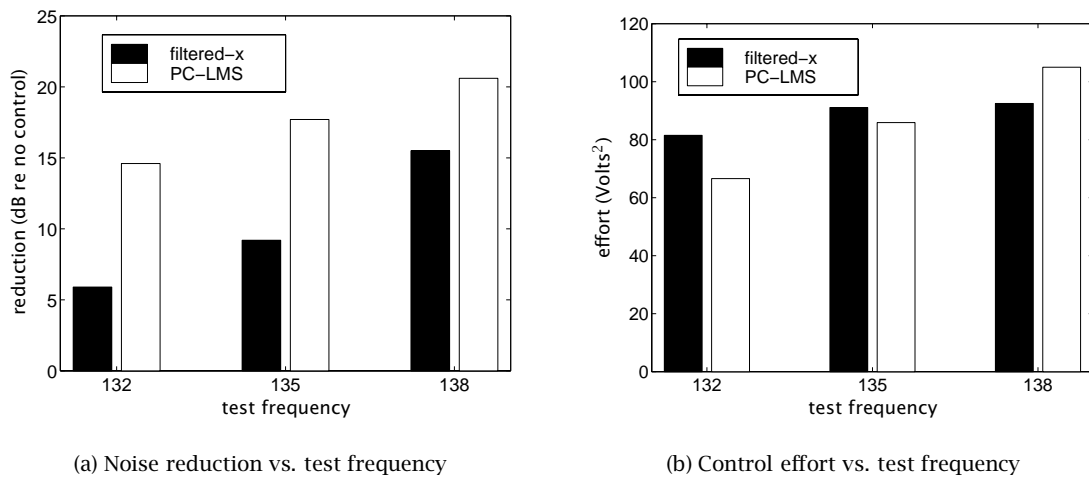


Figure 8.28: Noise reduction and total control effort for controller robustness test

## Chapter 9

# Conclusions

A principal component least mean square (PC-LMS) adaptive algorithm was described that addresses practical issues that arise when control is implemented on a complex structure with a large control system. The principal components of the transfer function matrix between sensors and actuators decouple the control system, so control can be implemented in terms of individual principal components. The resulting algorithm resembles transform domain adaptive algorithms that have been applied previously to single channel, broadband filtering problems. However, for the multichannel controller operating at a single frequency, the principal components represent a transformation based on spatial considerations rather than temporal properties.

Implementation of the PC-LMS algorithm consists of the following six steps:

1. the transfer function matrix between actuators and sensors at the single frequency of interest is measured
2. the singular value decomposition (SVD) is computed of the transfer function matrix in the frequency domain
3. the left singular vectors from the SVD correspond to transformation vectors that translate the error sensor responses into principal component responses
4. the right singular vectors correspond to transformation vectors that translate the actuator inputs into PC control inputs
5. because the left and right singular vectors are orthonormal, the transformation is easily reversed to go from PC coordinates to actuator or sensor coordinates
6. the control signals and updates to the control filter weights are computed in terms of the principal components of the control system

A theoretical analysis of the PC-LMS algorithm established the following advantages of implementing feedforward control using the principal components of the control system:

- the PC-LMS algorithm requires fewer computations per sample iteration to update the control filter weights than the filtered-x LMS algorithm

- the convergence of each PC is determined by an individual step size parameter, thus the convergence speed of the control filter weights can be individually varied. By proper selection of the step size parameters, the overall convergence can be as fast as Newton's algorithm. In addition, adaptation of an individual PC can be turned off by setting its step size parameter to zero.

The analysis also established the following properties of the PC-LMS algorithm:

- the robustness of convergence of the PC-LMS algorithm to errors in the transfer function matrix is identical to the robustness of the filtered-x LMS algorithm.
- the importance of each principal component in the control system can be quantified using the following metrics:
  - noise reduction obtained by each PC
  - effort required to cancel each PC
  - statistical significance of each PC in the presence of random sensor noise

Because the principal components are computed from a transfer function matrix between actuators and sensors at a single frequency, the sensitivity of the PCs to frequency variation was studied. Expressions for eigenvalue and eigenvector derivatives were used to compute the rate of change of the PCs. The derivatives were computed for the principal components of three dynamic systems: a simply supported plate, a simply supported plate radiating sound into a half space, and an enclosed cylindrical cavity. The principal components were found to vary smoothly for all three systems, although the phase changed significantly at the natural frequencies of the systems.

In order to compensate for the frequency variation of the principal components, a method for identifying the transfer function matrix while the controller is operating was described. This online identification method is suitable for a large control system, and relies on a random dither signal injected into the input to each control actuator. The dither signal creates a noise floor in the system that limits cost function reduction, but the advantage of adapting to the changing dynamics of the system can outweigh the disadvantage of the dither signal. A simulation of the online identification procedure demonstrated its usefulness for maintaining the stability of convergence of the PC-LMS algorithm when the reference frequency passed through a resonance of the dynamic system being controlled.

The theoretical studies of the PC-LMS algorithm were verified in a series of real-time experiments conducted on a closed cylindrical shell modeling an aircraft fuselage. The PC-LMS and filtered-x algorithms were programmed and executed on a digital signal processor residing in a desktop computer, which allowed real-time studies of the two algorithms. The control system consisted of 48 microphones uniformly distributed inside the shell, and 12 inertial force actuators mounted on the walls of the shell. Two loudspeakers were positioned on either side of the exterior of the shell and were used to create a primary disturbance sound field inside the shell. The performance of the PC-LMS and filtered-x LMS algorithms were compared at two test frequencies. The control algorithms were evaluated at 138 and 147 Hz, where 138 Hz was near a structural resonance and 147 Hz was close to a cavity resonance. When controlling all twelve PCs of the control system, the PC-LMS algorithm obtained noise reductions across all 48 microphones of 22.5 dB and 23.0 dB at 138 and 147 Hz, respectively. In contrast, the filtered-x LMS algorithm achieved only 12.2 dB and 21.1 dB at the same two frequencies.

The experiment demonstrated the advantages of implementing a control effort penalty by controlling only the well-conditioned PCs of the control system, in comparison to a uniform effort penalty in

the filtered-x LMS algorithm. For small effort penalties, the PC-LMS controller achieved higher noise reductions with the same or less control effort than the filtered-x LMS algorithm. Similar results were seen in a simple test concerning the robustness of the two adaptive algorithms to errors in the transfer function matrix; the PC-LMS controller produced greater noise reduction with less control effort than filtered-x LMS, as errors were introduced into the transfer function matrix.

It is recommended that future work be aimed at extending the PC-LMS algorithm to multiple frequencies, since a limitation of the current formulation is its restriction to single frequency control problems. A first step in this direction might be to develop the capability for the algorithm to track changes in the excitation frequency, since many practical control problems involve single frequency excitations that vary about a nominal value.

# Appendix A

## Analytical Models

This appendix describes the analytical models that were used to generate transfer functions from control actuators to error sensors at a single frequency for the control systems studied in Chapter 6. All of these models have been described elsewhere, but are included here for completeness. They are discussed in the same order as in Chapter 6: a simply supported vibrating plate; a plate radiating into an infinite half space; and a simply supported cylindrical shell with rigid end caps forming a closed cylindrical cavity.

### A.1 Vibrating plate

This section describes an analytical model for two dimensional bending waves in a simply supported plate. Consider the two dimensional plate and coordinate system shown in Fig. A.1. The classical bending wave equation for waves propagating in the  $x$  and  $z$  directions on the plate is written (Fahy 1985)

$$D \left( \frac{\partial^4 \eta}{\partial x^4} + 2 \frac{\partial^4 \eta}{\partial x^2 \partial y^2} + \frac{\partial^4 \eta}{\partial y^4} \right) = -m \frac{\partial^2 \eta}{\partial t^2} \quad (\text{A.1})$$

where  $m$  is the mass per unit length of the plate. The bending stiffness of the plate is

$$D = \frac{Eh^3}{12(1 - \nu^2)} \quad (\text{A.2})$$

where  $h$  is the plate thickness,  $\nu$  is Poisson's ratio, and  $E$  is Young's modulus. Structural damping in the plate is modeled by adding a small imaginary component to the modulus of elasticity, such that  $E' = E(1 + j\eta)$ , where  $\eta$  is the loss factor and is generally a small number (Fahy 1985).

Consider a candidate solution to the equation of motion, assuming harmonic motion, written

$$\psi(x, y, t) = \Psi e^{(i\omega t - k_x x - k_y y)} \quad (\text{A.3})$$

Substituting this into the equation of motion gives the dispersion relation

$$k_b = \left( \frac{m\omega^2}{D} \right)^{1/4} \quad (\text{A.4})$$

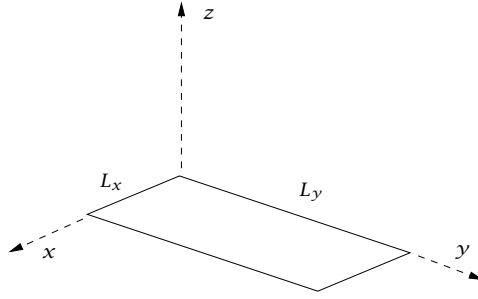


Figure A.1: Simply supported plate

where  $k_b^2 = k_x^2 + k_y^2$ .

Assuming the boundaries of the plate are simply supported, the boundary conditions are written as

$$\psi(0, y, t) = 0 \quad (\text{A.5})$$

$$\psi(x, 0, t) = 0 \quad (\text{A.6})$$

$$\frac{\partial^2 \psi}{\partial x^2} = 0 \quad (\text{A.7})$$

$$\frac{\partial^2 \psi}{\partial y^2} = 0 \quad (\text{A.8})$$

Applying these boundary conditions to the wave equation, the eigenfunctions for the system are found to be  $(\sin(k_x x) \sin(k_y y))$  where the wavenumbers are  $k_x = n_x \pi / L_x$ , and  $k_y = n_y \pi / L_y$ . By the expansion theorem (Meirovitch 1980), the system response can be written as

$$\psi(x, y, t) = \sum_{i=1}^{N_x} \sum_{j=1}^{N_y} A_{ij} \sin(k_x x) \sin(k_y y) \quad (\text{A.9})$$

$$= \sum_{n=1}^N A_n \psi_n(x, y) e^{i\omega t} \quad (\text{A.10})$$

The second equation is obtained by replacing the  $x$  and  $y$  modal indices with a single modal index  $n$ .

A solution for the forced response of the plate can be obtained if the eigenfunctions are substituted into a form of the equation of motion that includes an external forcing term. The equation of motion with the forcing term is written

$$D(\nabla^4 \psi) + m \frac{\partial^2 \psi}{\partial t^2} = F(x, y, t) \quad (\text{A.11})$$

Substituting the eigenfunction for the plate equation of motion, multiplying both sides by an eigenfunction  $\psi_m$  and integrating over the dimensions of the plate gives the result

$$(Dk_b^4 - \omega^2 m) \frac{L_x L_y}{4} A_n = F_n \quad (\text{A.12})$$

where  $F_n$ , the modal force is written as

$$F_n = \int_0^{L_x} \int_0^{L_y} F(x, y) \psi_m(x, y) dx dy \quad (\text{A.13})$$

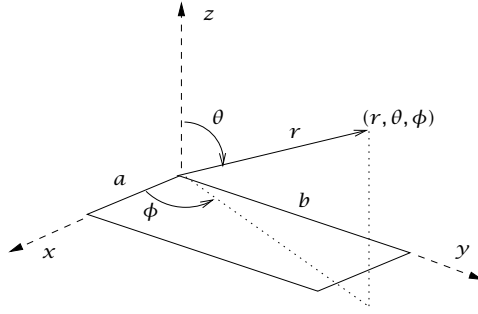


Figure A.2: Plate radiating into half space

The preceding equations can be used to determine the modal constants,  $A_n$ , for a given force distribution  $F(x, y)$ .

## A.2 Plate Sound Radiation

This section contains a description of the numerical model of a simply supported plate radiating sound into a half space. The details of the model are taken from Wallace (1972). Consider the two dimensional plate radiating into the half space above the  $x - y$  plate as shown in Fig. A.2. The fluid is assumed to be light, and hence fluid loading on the plate is neglected. As for the vibrating plate model, damping in the plate is modeled by adding a small imaginary component to the modulus of elasticity, such that  $E' = E(1 + j\eta)$ , where  $\eta$  is the loss factor and is generally a small number (Fahy 1985).

The Rayleigh integral will be used to compute the pressure at a point in the far field from the plate. This approach is valid for a planar surface, in which the pressure radiated from the entire plate is taken as the integral of contributions from elemental sources over surface of the plate. For a plate in a baffle, the pressure at a point in the far-field due to a velocity distribution  $u_\omega(x, y)$  on the plate is written as

$$p_\omega(r, \theta, \phi) = -ik\rho c \frac{e^{ikr}}{2\pi r} \times \int_0^b \int_0^a u_\omega(x, y) \exp \left[ -i \left( \frac{\alpha x}{a} \right) - i \left( \frac{\beta y}{b} \right) \right] dx dy \quad (\text{A.14})$$

where  $k$  and  $\rho c$  are characteristics of the fluid medium, and

$$\alpha = ka \sin \theta \cos \phi \quad (\text{A.15})$$

$$\beta = kb \sin \theta \sin \phi \quad (\text{A.16})$$

The time dependence of the pressure and velocity are understood to be  $e^{i\omega t}$ .

The surface velocity distribution for the rectangular plate can be written using the sin – sin eigenfunctions derived in the previous section. Using the coordinates from Fig. A.2 the  $m$ th eigenfunction is written

$$u_m(x, y) = U_m \sin \left( \frac{m\pi x}{a} \right) \sin \left( \frac{n\pi y}{b} \right) \quad (\text{A.17})$$

for  $x$  and  $y$  defined over the plate surface area. Substituting this equation into the expression for the Rayleigh integral yields (Wallace 1972)

$$p_{\omega}(r, \theta, \phi) = -iU_m k \rho c \frac{e^{ikr}}{2\pi r} \frac{ab}{mn\pi^2} \times \left[ \frac{(-1)^m e^{-i\alpha} - 1}{(\alpha/m\pi)^2 - 1} \right] \left[ \frac{(-1)^n e^{-i\beta} - 1}{(\beta/n\pi)^2 - 1} \right] \quad (\text{A.18})$$

The preceding expression can be used to compute the pressure at a point in the far field given a velocity distribution on the panel. The velocity distribution of the  $m$  mode due to a point force can be computed from Eqs. A.12 and A.13.

### A.3 Cylindrical Shell

The shell model used here is identical to the model described in Lester and Lefebvre (1993). The response of the cylindrical shell is modeled using the Donnell-Mushtari thin shell equations (Leissa 1973), which are the simplest class of thin shell equations. The acoustic response of the interior cavity is modeled using rigid-wall cylindrical modal basis functions. Modal coupling coefficients are used to relate the interior acoustic response to the response of the shell walls. The model is discussed here in terms of its constituent parts; first the Donnell-Mushtari cylinder equations are discussed, followed by the model for the interior acoustic space. The modal coupling coefficients between the two media are then described.

The nomenclature used in the following equations is given here.

Symbol	Description
$A_{mn}$	modal coefficient for $x$ component of force
$a$	radius of cylinder
$c_f$	speed of sound in air
$c_l$	axial phase speed in cylinder
$\hat{C}_{m'm}$	modal coupling coefficient
$E$	modulus of elasticity of cylinder
$F_{mn}$	modal coefficients for $x$ component of force
$F_c$	actuator complex amplitude
$f_x, f_{\theta}, f_r$	external forces acting on cylinder
$h$	cylinder thickness
$J_n$	complex Bessel function of order $n$
$k$	free space wave number, $= \omega/c_f$
$L$	length of cylinder
$m$	axial wave number
$n$	circumferential wave number
$P_{mn}$	modal coefficients for acoustic pressure in cylinder
$p$	acoustic pressure inside cylinder
$T_{mn}$	modal coefficients for $\theta$ component of force
$t$	time
$U_{mn}$	modal amplitudes for $u$ cylinder displacements
$u, v, w$	axial, circumferential, and radial cylinder displacements
$V_{mn}$	modal amplitudes for $v$ cylinder displacements

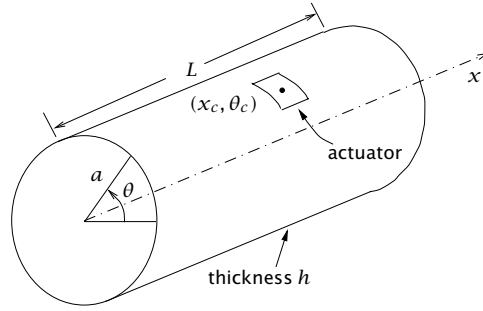


Figure A.3: Cylindrical coordinate system

(continued from previous page)

Symbol	Description
$W_{mn}$	modal amplitudes for $w$ cylinder displacements
$\mathbf{W}_{mn}$	modal coefficients for $w$
$x, r, \theta$	cylindrical coordinates
$x_c, \theta_c$	coordinates of center of actuator
$\alpha_m$	radial wave number
$\Delta x, \Delta \theta$	dimensions of PZT patch
$\epsilon_m$	equals 2 if $m = 0$ , equals 1 otherwise
$\nu$	Poisson's ratio
$\rho_f$	density of air
$\rho_s$	density of cylinder
$\Omega$	non-dimensional frequency, $\Omega = \omega a / c_l$
$\omega$	circular frequency

In addition, the superscripts  $s$  and  $c$  on modal coefficients denote coefficients of the sin and cosine terms, respectively.

### A.3.1 Cylinder Equations

This description of the cylinder equations follows the description given in the Appendix of Lester and Lefebvre (1993). The coordinate system is shown in Fig. A.3.

The equations of motion for each coordinate on the middle surface of the shell wall are given by the Donnell-Mushtari cylinder equations which are written as follows:

$$\left(\frac{1}{c_l^2}\right) \frac{\partial^2 u}{\partial t^2} - \frac{\partial^2 u}{\partial x^2} - \left(\frac{1-\nu}{2a^2}\right) \frac{\partial^2 u}{\partial \theta^2} - \left(\frac{1+\nu}{2a}\right) \frac{\partial^2 v}{\partial x \partial \theta} - \left(\frac{\nu}{a}\right) \frac{\partial w}{\partial x} = \left(\frac{1-\nu^2}{Eh}\right) f_x \quad (\text{A.19})$$

$$\left(\frac{1}{c_l^2}\right) \frac{\partial^2 v}{\partial t^2} - \left(\frac{1+\nu}{2a}\right) \frac{\partial^2 u}{\partial x \partial \theta} - \left(\frac{1-\nu}{2}\right) \frac{\partial^2 v}{\partial x^2} - \left(\frac{1}{a^2}\right) \frac{\partial^2 v}{\partial \theta^2} - \left(\frac{1}{a^2}\right) \frac{\partial w}{\partial \theta} = \left(\frac{1-\nu^2}{Eh}\right) f_\theta \quad (\text{A.20})$$

$$\left(\frac{1}{c_l^2}\right) \frac{\partial^2 w}{\partial t^2} - \left(\frac{\nu}{a}\right) \frac{\partial u}{\partial x} - \left(\frac{1}{a^2}\right) \frac{\partial v}{\partial \theta} + \left(\frac{1}{a^2}\right) w + \left(\frac{h^2}{12}\right) \nabla_w^4 = - \left(\frac{1-\nu^2}{Eh}\right) f_r \quad (\text{A.21})$$

The axial phase speed in the shell is given by the equation

$$c_l = \left[ \frac{E}{\rho_s(1-\nu^2)} \right]^{1/2} \quad (\text{A.22})$$

The steady state displacement of the simply supported cylinder can be expressed in terms of the modal basis functions:

$$u(x, \theta) = \sum_{n=0} \sum_{m=0} \cos\left(\frac{m\pi x}{L}\right) [U_{mn}^c \cos(n\theta) + U_{mn}^s \sin(n\theta)] \quad (\text{A.23})$$

$$v(x, \theta) = \sum_{n=0} \sum_{m=1} \sin\left(\frac{m\pi x}{L}\right) [V_{mn}^c \cos(n\theta) + V_{mn}^s \sin(n\theta)] \quad (\text{A.24})$$

$$w(x, \theta) = \sum_{n=0} \sum_{m=1} \sin\left(\frac{m\pi x}{L}\right) [W_{mn}^c \cos(n\theta) + W_{mn}^s \sin(n\theta)] \quad (\text{A.25})$$

The forces induced by the PZT actuators are represented by the three components,  $f_x, f_\theta, f_r$ . The forces are assumed to act on the middle surface of the shell and are expressed in terms of force per unit area. A harmonic time variation is assumed for all forces. The control force acting on the shell can be represented by a modal expansion similar to that used for the displacements, as:

$$f_x(x, \theta) = \sum_{n=0} \sum_{m=0} \cos\left(\frac{m\pi x}{L}\right) [A_{mn}^c \cos(n\theta) + A_{mn}^s \sin(n\theta)] \quad (\text{A.26})$$

$$f_\theta(x, \theta) = \sum_{n=0} \sum_{m=1} \sin\left(\frac{m\pi x}{L}\right) [T_{mn}^c \cos(n\theta) + T_{mn}^s \sin(n\theta)] \quad (\text{A.27})$$

$$f_r(x, \theta) = \sum_{n=0} \sum_{m=1} \sin\left(\frac{m\pi x}{L}\right) [F_{mn}^c \cos(n\theta) + F_{mn}^s \sin(n\theta)] \quad (\text{A.28})$$

The external forces are assumed to be produced by pairs of PZT patches located on the shell walls. The patches are driven in phase with one another and as a result produce an in-plane stress distribution in the shell. Hence, the radial component of the force due to a patch is zero, i.e.,  $f_r(x, \theta) = 0$ . Using standard modal expansion techniques, the modal coefficients in the equations for the force component in the  $x$  direction,  $f_x(x, \theta)$ , are given by:

$$A_{mn}^c = \frac{-8F_c}{\pi L} \sin\left(\frac{m\pi\Delta x}{2L}\right) \sin\left(\frac{m\pi x_c}{L}\right) \begin{cases} \frac{\Delta\theta}{4} & \text{if } n = 0 \\ \frac{1}{n} \sin\left(\frac{n\Delta\theta}{2}\right) \cos(n\theta_c) & \text{otherwise} \end{cases} \quad (\text{A.29})$$

$$A_{mn}^s = \frac{-8F_c}{\pi L} \sin\left(\frac{m\pi\Delta x}{2L}\right) \sin\left(\frac{m\pi x_c}{L}\right) \begin{cases} 0 & \text{if } n = 0 \\ \frac{1}{n} \sin\left(\frac{n\Delta\theta}{2}\right) \sin(n\theta_c) & \text{otherwise} \end{cases} \quad (\text{A.30})$$

The modal coefficients for the force component in the  $\theta$  direction,  $f_\theta(x, \theta)$ , are given by:

$$T_{mn}^c = \frac{-8F_c}{\pi^2 a} \sin\left(\frac{m\pi\Delta x}{2L}\right) \sin\left(\frac{m\pi x_c}{L}\right) \begin{cases} 0 & \text{if } n = 0 \\ \frac{1}{m} \sin\left(\frac{n\Delta\theta}{2}\right) \cos(n\theta_c) & \text{otherwise} \end{cases} \quad (\text{A.31})$$

$$T_{mn}^s = \frac{8F_c}{\pi^2 a} \sin\left(\frac{m\pi\Delta x}{2L}\right) \sin\left(\frac{m\pi x_c}{L}\right) \begin{cases} 0 & \text{if } n = 0 \\ \frac{1}{m} \sin\left(\frac{n\Delta\theta}{2}\right) \sin(n\theta_c) & \text{otherwise} \end{cases} \quad (\text{A.32})$$

The acoustic response inside the cylinder is determined only by radial displacements of the shell, hence only the displacement  $w(x, \theta, t)$  in Eq. A.25 needs to be computed. The modal coefficients,  $W_{mn}^c$  and  $W_{mn}^s$ , can be determined from the coefficients  $A_{mn}^c, A_{mn}^s, T_{mn}^c$ , and  $T_{mn}^s$  on a mode by mode basis.

### A.3.2 Interior Acoustic Response

The response of the interior cavity is represented in terms of modal basis functions for a rigid-wall cylindrical shell. Once again, the derivation here follows that given in Lester and Lefebvre (1993). The pressure at a point inside the shell is written

$$p(x, r, \theta) = \sum_{n=0} \sum_{m=0} J_n(\alpha_m r) \cos\left(\frac{m\pi x}{L}\right) [P_{mn}^c \cos(n\theta) + P_{mn}^s \sin(n\theta)] \quad (\text{A.33})$$

where the radial wave number is written in terms of the acoustic wave number and the axial wave number as

$$\alpha_m^2 = k^2 - \left(\frac{m\pi}{L}\right)^2 \quad (\text{A.34})$$

The coefficients in Eq. A.33 can be determined by satisfying the momentum boundary condition at the interior cylinder wall. This boundary condition is written

$$\rho_f \omega^2 w(x, \theta) = \frac{\partial p(x, a, \theta)}{\partial r} \quad (\text{A.35})$$

where the derivative of the interior acoustic pressure is evaluated on the cylinder wall, at  $r = a$ .

However, before this boundary condition can be applied, the cylinder displacement in Eq. A.25, which is written in terms of sine basis functions, must be rewritten in terms of cosine basis functions to match the basis functions used to describe the acoustic pressure in Eq. A.35. That is, the radial displacement of the cylinder is rewritten in terms of cosine functions as

$$w(x, \theta) = \sum_{n=0} \sum_{m=1} \cos\left(\frac{m\pi x}{L}\right) [\hat{W}_{mn}^c \cos(n\theta) + \hat{W}_{mn}^s \sin(n\theta)] \quad (\text{A.36})$$

The modal amplitudes in this equation can be determined from the modal amplitudes in Eq. A.25 using modal coupling coefficients as

$$\hat{W}_{mn}^c = \sum_{m'=1} \hat{C}_{m'm} W_{m'n}^c \quad (\text{A.37})$$

$$\hat{W}_{mn}^s = \sum_{m'=1} \hat{C}_{m'm} W_{m'n}^s \quad (\text{A.38})$$

where  $\hat{C}_{m'm}$  is the modal coupling coefficient. The coupling coefficients are calculated as

$$\hat{C}_{m'm} = \begin{cases} \Delta_{m'm}^{(-)} + \Delta_{m'm}^{(+)} & \text{if } m' \neq m \\ 0 & \text{otherwise} \end{cases} \quad (\text{A.39})$$

$$(\text{A.40})$$

$$\Delta_{m'm}^{(\pm)} = \frac{1}{\pi \epsilon_m} \left[ \frac{1 - \cos(m' \pm m)\pi}{m' \pm m} \right] \quad (\text{A.41})$$

This coupling term couples the cylinder and acoustic responses through the respective axial wave numbers,  $m'$  and  $m$ , for each domain. There is assumed to be no modal cross coupling between circumferential wave numbers,  $n$ .

The expression for the acoustic pressure in Eq. A.33 requires computation of modal pressure coefficients as follows:

$$P_{mn}^c = P_{mn}(\omega) \hat{W}_{mn}^c \quad (\text{A.42})$$

$$P_{mn}^s = P_{mn}(\omega) \hat{W}_{mn}^s \quad (\text{A.43})$$

The term  $P_{mn}(\omega)$  relates the acoustic cavity mode amplitudes to the amplitudes of the cosine cylinder displacement modes, and the cosine cylinder displacement amplitudes are related to the sine cylinder displacement amplitudes by the modal coupling coefficient,  $\hat{C}_{m'm}$ . The modal transfer function from cylinder cosine displacements to acoustic cavity mode amplitudes is given by

$$P_{mn}(\omega) = \frac{\rho_f \omega^2}{\alpha_n J'_n(\alpha_n a)} \quad (\text{A.44})$$

## Appendix B

# Online Identification Simulation Code

This chapter contains MATLAB code used for the PC-LMS controller simulation with online system identification. MATLAB is a commercial software tool that is useful for manipulating vectors and matrices. The code listed here uses features of MATLAB version 5.0, which was released in early 1997.

The simulation code loads in data containing a state space representation of the system being modeled, in the frequency range of interest. For the results discussed in Chapter 7, a model of a simply supported plate was created.

The code listing here has been broken up into sections. Comments appropriate for each section have been added here to improve the readability of the code.

```
%%%%%%%%%%%%%%%%%%%%%%%%%%%%%%%%%%%%%%%%%%%%%%%%%%%%%%%%%%%%%%%%%%%%%%%%%%
% Define some constants
% - snr is signal to noise ratio of sensor noise
% - transient_cycles is time for sys to reach steady state
% - run_cycles is total number of cycles to run controller
% - flip_cycles is how often to change the state
%   space matrices
%%%%%%%%%%%%%%%%%%%%%%%%%%%%%%%%%%%%%%%%%%%%%%%%%%%%%%%%%%%%%%%%%%%%%%%%%%
samp_per_cycle = 10;
snr            = 60;
mu            = 10;
navg_control_on = 15;
run_cycles    = 10000;
navg_flip_sys = 93;
leak_factor   = 0.99;
dither_amp    = 0.01;
fft_mult      = 50;
transient_cycles = 50;
primary_actuator = 1;
ssindex       = 1;
```

This initial section of code defines numerous constants that usually change from run to run. Most variables are either self explanatory or are described in the code comments. Other variables are:

**ssindex** a counter denoting which of the 6 state space models is being used in the simulation



```

% Create system-id related variables
%%%%%%%%%%%%%%%%%%%%%%%%%%%%%%%%%%%%%%%%%%%%%%%%%%%%%%%%%%%%%%%%%%%%%%%%
fft_length = fft_mult*samp_per_cycle;
n = (0:fft_length-1)';
c0 = cos(2*pi*n/samp_per_cycle);
s0 = sin(2*pi*n/samp_per_cycle);

Xf = zeros(r,1);
Yf = zeros(m,1);

Gij = zeros(r,r);
Giy = zeros(m,r);
Hhat = zeros(m,r);

x = zeros(r,1);
xsave = zeros(r,fft_length);
ysave = zeros(m,fft_length);

```

The primary disturbance input is applied to the state space model for a short time here in order to allow the state vector to reach steady state. The response level is used to compute the amplitude of the measurement noise term in order to achieve the signal to noise ratio set in the constant snr.

```

%%%%%%%%%%%%%%%%%%%%%%%%%%%%%%%%%%%%%%%%%%%%%%%%%%%%%%%%%%%%%%%%%%%%%%%%
% Start up system to reach steady state
% - compute ms Y for noise_amp calculation
%%%%%%%%%%%%%%%%%%%%%%%%%%%%%%%%%%%%%%%%%%%%%%%%%%%%%%%%%%%%%%%%%%%%%%%%
ytemp = zeros(m,transient_pts);
for ii=1:transient_pts,
    U(primary_actuator,1) = sin(2*pi*ii/samp_per_cycle);
    ytemp(:,ii) = Ca(:, :,ssindex)*X + Da(:, :,ssindex)*U;
    X = Aa(:, :,ssindex)*X + Ba(:, :,ssindex)*U;
end
ytemp = ytemp(:,(transient_pts-2*samp_per_cycle):transient_pts);
ytemp = ytemp.*ytemp;
rmsy = sqrt(mean(mean(ytemp)));

%%%%%%%%%%%%%%%%%%%%%%%%%%%%%%%%%%%%%%%%%%%%%%%%%%%%%%%%%%%%%%%%%%%%%%%%
% Compute amplitude of random noise
%%%%%%%%%%%%%%%%%%%%%%%%%%%%%%%%%%%%%%%%%%%%%%%%%%%%%%%%%%%%%%%%%%%%%%%%
noise_amp = 2*(rmsy/(10^(snr/20)))/0.3333;

```

This is the main iteration loop; each time through the loop represents a single sample interval. The counter variable `fft_count` keeps track of accumulated products in the Fourier transform computation. The number of completed transforms is counted by `navg`. This variable determines when control is turned on and when the state space matrix index is incremented.

```

%%%%%%%%%%%%%%%%%%%%%%%%%%%%%%%%%%%%%%%%%%%%%%%%%%%%%%%%%%%%%%%%%%%%%%%%
%%%%%%%%%%%%%%%%%%%%%%%%%%%%%%%%%%%%%%%%%%%%%%%%%%%%%%%%%%%%%%%%%%%%%%%%
% Begin main iteration loop
%%%%%%%%%%%%%%%%%%%%%%%%%%%%%%%%%%%%%%%%%%%%%%%%%%%%%%%%%%%%%%%%%%%%%%%%
%%%%%%%%%%%%%%%%%%%%%%%%%%%%%%%%%%%%%%%%%%%%%%%%%%%%%%%%%%%%%%%%%%%%%%%%
fft_count = 1;
navg = 0;
flip_count = 0;

```

```

for ii=1:run_pts,
    if ~rem(ii,500), ii, end

    %%%%%%%%%%%
    % Update reference input vector
    %%%%%%%%%%%
    xtemp(1) = xtemp(2);
    xtemp(2) = sin(2*pi*ii/samp_per_cycle);

```

The actuator inputs are calculated here. The first actuator corresponds to the primary disturbance actuator, and hence its input consists of a sinusoid. The other actuators are used for control and hence have random dither added to their inputs here. The control inputs are computed first in PC coordinates, then transformed into actuator coordinates.

```

%%%%%%%%%%
% Set actuator inputs
%%%%%%%%%%
U = [xtemp(2); dither_amp*2*(rand(3,1)-0.5)];
pc_control(:,1) = pc_control(:,2);
pc_control(:,2) = w*xtemp;

for jj=1:n_control,
    U(2:4,1) = U(2:4,1) + vpc(:, :, jj)*pc_control(jj, :);
end

```

The actuator inputs are propagated through the state space model. Note how `ssindex` is used to index through the matrix of state space models.

```

%%%%%%%%%%
% Propagate thru ss model
%%%%%%%%%%
Y = Ca(:, :, ssindex)*X + Da(:, :, ssindex)*U;
X = Aa(:, :, ssindex)*X + Ba(:, :, ssindex)*U;

%%%%%%%%%%
% Add in sensor noise here
%%%%%%%%%%
Y = Y + noise_amp*(rand(m,1)-0.5);

```

After measurement noise is added to the sensors, the online id is updated here. To save computation time in MATLAB, temporary matrices `xsave` and `ysave` are filled in with `fft_length` input ( $x$ ) and output ( $y$ ) values. Once full, these matrices are multiplied by `c0` and `s0` to obtain the Fourier transforms of the records at the excitation frequency.

The matrices containing spectral densities,  $G_{ij}$  and  $G_{iy}$ , are updated here with leaky averaging filters. If the initial startup period has been exceeded (`navg_control_on`) then the transfer function is computed ( $\hat{H}$ ). The PCs are then computed from this matrix using the MATLAB singular value decomposition routine. The resulting singular vectors  $u$  and  $v$  are transformed from the frequency domain to the time domain.

```

%% Update system id
xsave(:,fft_count) = U;
ysave(:,fft_count) = Y;
fft_count = fft_count + 1;
if (fft_count > fft_length),
    fft_count = 1;
    Xf = xsave*c0 - i*xsave*s0;
    Yf = ysave*c0 - i*ysave*s0;
    Gij = leak_factor*Gij + (1-leak_factor)*(Xf*Xf');
    Giy = leak_factor*Giy + (1-leak_factor)*(Yf*Xf');
    navg = navg + 1;

    if (navg >= navg_control_on),
        pcmu = mu*[1;0;0];
        Hhat = Giy/Gij;
        [u,s,v] = svd(Hhat(:,2:4));
        for jj=1:n_control,
            upc(:,,jj) = f2t(conj(u(:,jj)),deltat);
            vpc(:,,jj) = f2t(v(:,jj),deltat);
        end

        flip_count = flip_count + 1;
        if (flip_count >= navg_flip_sys ),
            flip_count = 0;
            ssindex = ssindex + 1;
        end
        if(ssindex > 6), ssindex = 6; end
    end
end
end

```

This last section of code is the LMS algorithm in PC coordinates. First, the sensor responses in  $Y$  are transformed to PC coordinates. The resulting vector of PC errors,  $pc\_error$ , is then used to update the control filter weights in  $w$ .

```

%% Compute PC error terms
e(:,1) = e(:,2);
e(:,2) = Y;
esave(ii,1) = Y'*Y;
for jj=1:n_control,
    pc_error(jj) = upc(:,1,jj)'*e(:,1) + upc(:,2,jj)'*e(:,2);
end

%% Update PC control weights
w(:,1) = w(:,1) - pcmu .* pc_error * xtemp(1);
w(:,2) = w(:,2) - pcmu .* pc_error * xtemp(2);

wsave(ii,:) = w(1,:);

end

```

## Appendix C

# Principal Component Analysis as a Control Design Tool

Although this thesis has discussed the implementation of feedforward control using the principal components of the control system, the PCs can also be used to design the control system. The shapes of the singular vectors at the error sensors and control actuators can provide insight into how to optimally group actuators or sensors, thereby simplifying the control system. This appendix contains a brief description of a control application where the shapes of the PCs at the actuators suggest how to hardwire the actuator inputs together and avoid ill-conditioning problems.

The application concerns the active control of sound radiated from the inlet of a turbofan engine. Control actuators are mounted on the interior circumference of the inlet in a symmetric arrangement. This actuator arrangement is needed in order to produce spinning duct modes for controlling the noise radiated by a fan in the duct. However, the symmetry of the actuator arrangement creates an ill-conditioned control system. If the actuators are hard-wired together and treated as a single degree of freedom in the control system, the ill-conditioning can be avoided. The principal components of the control system can offer insight into how to optimally hardwire the actuators together.

The active control of noise radiated from the inlet of a turbofan engine has been described previously (Thomas et al. 1994; Risi and Burdisso 1994). The goal is to reduce tonal noise created by the fan that radiates out the engine inlet. Control is applied with acoustic sources mounted around the circumference of the inlet, and the error sensors are microphones positioned outside the inlet. A simple schematic of this control arrangement is shown in Fig. C.1. Previous work has developed an analytical model to study control of the inlet radiation problem (Risi and Burdisso 1994). This analytical model was used to generate transfer function matrices for a prototypical control system, and the principal components of the transfer function matrix at a single frequency were studied.

The control system consists of twelve acoustic point sources mounted at a constant axial location 0.15 m from the opening of the duct. The sources were uniformly distributed around the circumference of the duct. In the analytical model, the control sources coupled into the first 15 duct modes that were cut-on at the test frequency of 2400 Hz. The primary source was modeled as a piston 1 m from the duct opening, and the piston generated only the (1,0), (1,1), and (1,2) duct modes. Two hundred and seventy six microphones were arranged uniformly on a hemispherical surface outside the duct as error sensors. This is many more microphones than would be used in an actual control system, but the large number was used to accurately estimate sound power radiated from the duct.

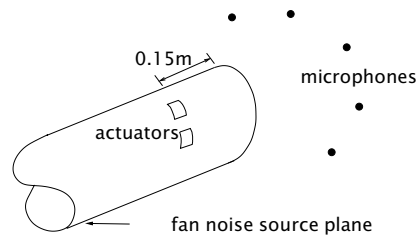


Figure C.1: Schematic of control system for turbofan noise

Table C.1: Properties of principal components

PC number	singular value	noise reduction (dB)
1	1.25	3.1E-06
2	1.25	2.8E-06
3	1.16	1.7E-07
4	1.15	1.4E-08
5	1.09	6.5E-07
6	0.95	6.6E-06
7	0.94	5.4E-05
8	0.93	1.5
9	0.93	1.5
10	0.86	1.3E-04
11	0.86	7.4E-05
12	0.00	2.1E-07

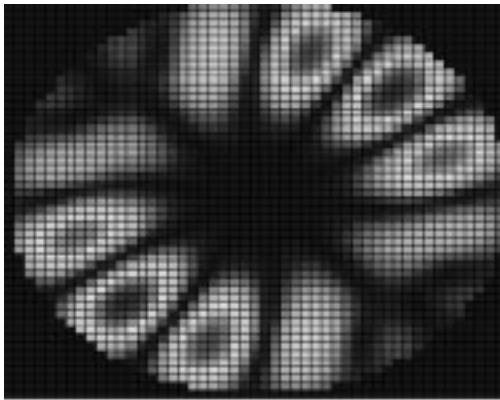
The transfer function matrix and primary response vector at 2400 Hz were generated using the analytical model described in Risi and Burdisso (1994). Properties of the principal components of the control system at 2400 Hz are listed in Table C.1. The second column lists the singular values for each principal component. Several pairs of PCs in the table have identical singular values. This is a result of the symmetry in the control system; both principal components in the pair create the same radiation pattern at the error sensors, except one is rotated by  $90^\circ$  relative to the other. The radiation patterns corresponding to such a pair of PCs are therefore orthogonal, and the equal singular values indicate the two PCs contribute equally to the transfer function matrix. The last singular value is zero, which indicates the control system is ill-conditioned at this frequency and an effort penalty or PC-LMS algorithm would have to be used to successfully implement control. The noise reduction corresponding to each PC is listed in the last column in Table C.1, and only the eighth and ninth principal components produce appreciable noise reduction.

The optimum control inputs to the twelve actuators are listed in Table C.2. With these inputs, the primary noise field is reduced by 3.8 dB at the error sensors. The magnitudes of the inputs are normalized relative to the maximum control input, and the values in the table indicates the actuators were driven with the same magnitude control signal. The control inputs to the actuators are phased to produce a spinning first order circumferential mode in the duct. The inputs to actuators on opposite sides of the duct (e.g., 1-7, 2-8, 3-9) are phased  $180^\circ$  apart, which will produce a first order circumferential mode in the duct. The phasing between neighboring actuators creates a spinning mode in the duct. This control field is to be expected since the primary noise field consisted of only first order circumferential modes.

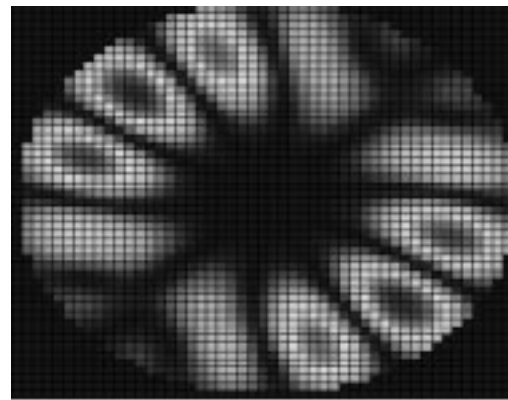
The left singular vectors (columns of  $U$ ) corresponding to the shapes of the PCs at the error sensors

Table C.2: Optimum actuator inputs

Actuator	Normalized magnitude	Phase (degrees)
1	0.98	30.1
2	1.00	61.0
3	1.00	89.7
4	0.98	120.4
5	0.99	151.0
6	1.00	179.9
7	0.99	-149.8
8	0.99	-119.4
9	0.99	-90.0
10	0.99	-59.1
11	1.00	-29.2
12	0.99	-0.24



(a) first PC at error sensors

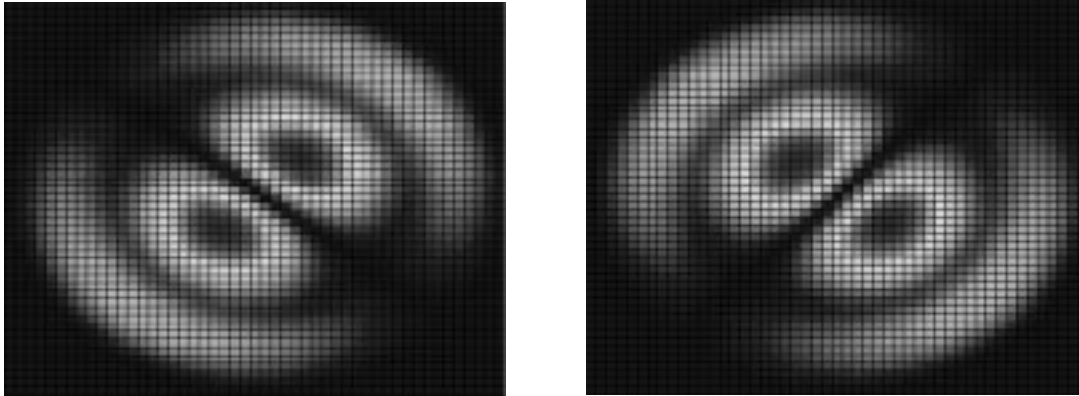


(b) second PC at error sensors

Figure C.2: First and second left singular vectors

for PCs 1,2, 8 and 9 are plotted in Figs. C.2 and C.3. The plots are shown from the perspective of looking into the engine inlet, onto the hemispherical surface containing the microphones. The first and second PC PCs resemble the radiation from a fifth order circumferential duct mode. The shape of the second PC is nearly identical to the first PC, except for a rotation of  $90^\circ$ . If these two PCs are driven with the proper phasing, a spinning fifth order circumferential duct mode can be excited. The eighth and ninth PCs, shown in Fig. C.3, have a similar relationship. These two PCs are associated with a first order circumferential duct mode. The primary noise source excites only first order circumferential modes, hence PCs eight and nine are useful for reducing the radiated sound field, as indicated in Table C.1.

The actuator inputs contained in the right singular vectors of the eighth and ninth PCs describe the input phasing for exciting the first order circumferential mode in the duct. These inputs correspond to those listed in Table C.2. Hence, the actuator inputs can be hardwired together using the phasing specified in the table in order to insure the control system excites a first order circumferential duct mode. This actuator arrangement can then be treated as a single control channel whose amplitude



(a) eighth PC at error sensors

(b) ninth PC at error sensors

Figure C.3: Eighth and ninth left singular vectors

and phase is optimized for a particular primary response field. This illustrates how the principal components of a control system can be used to determine an optimal actuator grouping that is then hardwired into the control system. For the turbofan inlet control problem, the actuator grouping can be easily related to the dynamics of the inlet sound radiation problem.

However, a static grouping of the actuators or sensors is not likely to be optimal at all operating conditions of the controller. In most control systems, the optimal groupings will depend on the transfer function matrix of the control system. This limitation of static groupings was a motivation for the work described in this thesis. If the PCs are used internally to the control algorithm to group the actuators and sensors, the actuator/sensor groupings can easily be reconfigured online as the dynamics of the system change.

# Bibliography

- Baumann, W. T., W. R. Saunders, and H. H. Robertshaw (1991, December). Active suppression of acoustic radiation from impulsively excited structures. *Journal of the Acoustical Society of America* 90(6), 3202-3208.
- Beaufays, F. (1995). Transform-domain adaptive filters: An analytical approach. *IEEE Transactions on Signal Processing* 43(2), 422-431.
- Bendat, J. S. and A. G. Piersol (1986). *Random Data* (Second ed.). New York: Wiley-Interscience.
- Blevins, R. D. (1984). *Formulas for Natural Frequency and Mode Shape*. Malabar, Florida: Krieger Publishing.
- Bouchard, M. and B. Paillard (1996, November). A transform domain optimization to increase the convergence speed of the multichannel filtered-x least-mean-square algorithm. *Journal of the Acoustical Society of America* 100(5), 3203-3214.
- Boucher, C., S. Elliott, and P. Nelson (1991, April). The effects of modelling errors on the performance and stability of active noise control systems. In *First Conference on Recent Advances in Active Control of Sound and Vibration*, Blacksburg, Virginia, pp. 290-301.
- Bronzel, M. J. and C. R. Fuller (1995, July). Implementation of fast recursive estimation techniques for active control of structural sound radiation. In *Active 95, Newport Beach, CA, July 6-9, 1995*, Newport Beach, pp. 359-368.
- Bullmore, A. J., P. A. Nelson, and S. J. Elliott (1990). Theoretical studies of the active control of propeller-induced cabin noise. *Journal of Sound and Vibration* 140(2), 191-217.
- Bullmore, A. J., P. A. Nelson, S. J. Elliott, J. F. Evers, and B. Chidley (1987, October). Models for evaluating the performance of propeller aircraft active noise control systems. In *AIAA 11th Aeroacoustics Conference, Palo Alto, CA, October 19-21, 1987*, Number AIAA 87-2704.
- Burdisso, R. A. and C. R. Fuller (1994, September). Design of active structural acoustic control systems by eigenproperty assignment. *Journal of the Acoustical Society of America* 96(3), 1582-1591.
- Burgess, J. C. (1981, September). Active adaptive sound control in a duct: A computer simulation. *Journal of the Acoustical Society of America* 70(3), 715-726.
- C. Bao, P. Sas, H. V. B. (1993a, Feb-Mar). Adaptive active control of noise in 3-d reverberant enclosures. *Journal of Sound and Vibration* 161, 501-514.
- C. Bao, P. Sas, H. V. B. (1993b, April). Comparison of two on-line identification algorithms for active noise control. In *Second Conference on Recent Advances in Active Control of Sound and Vibration*, Blacksburg, Virginia, pp. 38-51.
- Cabell, R. H., H. C. Lester, G. P. Mathur, and B. N. Tran (1993, October). Optimization of actuator arrays for aircraft interior noise control. In *AIAA 15th Aeroacoustics Conference, Long Beach, CA, October 25-27, 1993*, Number AIAA 93-4447.

- Cabell, R. H., H. C. Lester, and R. J. Silcox (1992, June). The optimization of force inputs for active structural acoustic control using a neural network. Technical Report 107627, NASA.
- Cabell, R. H., G. C. Smith, and C. R. Fuller (1995, July). Experimental investigation of actuator grouping for active structural acoustic control. In *Active 95, Newport Beach, CA, July 6-9, 1995*, Newport Beach, pp. 347-358.
- Clark, R. L. (1995). Adaptive feedforward modal space control. *Journal of the Acoustical Society of America* 98(5), 2639-2650.
- Cowan, C. and P. Grant (1985). *Adaptive Filters*. Prentice Hall.
- Cunefare, K. A. (1991). The minimum multimodal radiation efficiency of baffled finite beams. *Journal of the Acoustical Society of America* 90(5), 2521-2529.
- Cunefare, K. A. (1992, December). Effect of modal interaction on sound radiation from vibrating structures. *AIAA Journal* 30(12), 2819-2828.
- Dorling, C., G. Eatwell, S. Hutchins, C. Ross, and S. Sutcliffe (1989). A demonstration of active noise reduction in an aircraft cabin. *Journal of Sound and Vibration* 128, 358-360.
- Draper, N. and H. Smith (1981). *Applied Regression Analysis* (2nd ed.). John Wiley and Sons.
- Elliott, S. J., C. C. Boucher, and P. A. Nelson (1992, May). The behavior of a multiple channel active control system. *IEEE Transactions on Signal Processing* 40(5), 1041-1052.
- Elliott, S. J. and M. E. Johnson (1993, October). Radiation modes and the active control of sound power. *Journal of the Acoustical Society of America* 94(4), 2194-2204.
- Elliott, S. J. and P. Nelson (1993, October). Active noise control. *IEEE Signal Processing Magazine*, 12-35.
- Elliott, S. J., P. A. Nelson, I. M. Stothers, and C. C. Boucher (1989). Preliminary results of in-flight experiments on the active control of propeller-induced cabin noise. *Journal of Sound and Vibration* 128(2), 355-357.
- Elliott, S. J., P. A. Nelson, I. M. Stothers, and C. C. Boucher (1990). In-flight experiments on the active control of propeller-induced cabin noise. *Journal of Sound and Vibration* 140(2), 219-238.
- Elliott, S. J., I. M. Stothers, and P. A. Nelson (1987, October). A multiple error lms algorithm and its application to the active control of sound and vibration. *IEEE Transactions on Acoustics, Speech, and Signal Processing ASSP-35*(10), 1423-1434.
- Eriksson, L. and M. Allie (1989, February). Use of random noise for on-line transducer modeling in an adaptive active attenuation system. *Journal of the Acoustical Society of America* 85(2), 797-802.
- Fahy, F. (1985). *Sound and Structural Vibration: Radiation, Transmission, and Response*. Academic Press.
- Feintuch, P. L., N. J. Bershad, and A. K. Lo (1993, April). A frequency domain model for 'filtered' lms algorithms - stability analysis, design, and elimination of the training mode. *IEEE Transactions on Signal Processing* 41(4), 1518-1531.
- Ferrara, E. R. (1980, August). Fast implementation of lms adaptive filters. *IEEE Transactions on Acoustics, Speech, and Signal Processing ASSP-28*(4), 474-475.
- Fuller, C. (1987). Apparatus and method for global noise reduction. U.S. Patent No. 4715599.
- Fuller, C. and J. Carneal (1993, June). A biologically inspired control approach for distributed elastic systems. *Journal of the Acoustical Society of America* 93(6), 3511-3513.
- Fuller, C., S. Elliott, and P. Nelson (1996). *Active Control of Vibration*. Academic Press.
- Fuller, C. R. and F. J. Fahy (1982). Characteristics of wave propagation and energy distributions in cylindrical elastic shells filled with fluid. *Journal of Sound and Vibration* 81(4), 501-518.

- Fuller, C. R. and J. D. Jones (1987). Experiments on reduction of propeller induced interior noise by active control of cylinder vibration. *Journal of Sound and Vibration* 112, 389–395.
- Gibbs, G., S. Paxton, and C. Fuller (1997, January). An experimental based actuator optimization scheme for active structural acoustic control of interior noise in aircraft. In *Proceedings of the Fifth Pan American Congress of Applied Mechanics, San Juan, Puerto Rico*, pp. 407–411.
- Grosveld, F. and T. Beyer (1986, July). Modal characteristics of a stiffened composite cylinder with open and closed end conditions. In *AIAA 10th Aeroacoustics Conference, Seattle, WA, July 9–11, 1986*, Number AIAA 86-1908. AIAA.
- Grosveld, F. W. and H. C. Lester (1995, July). Numerical study of active sound transmission control for stiffened double wall cylinders. In *Active 95, Newport Beach, CA, July 6–9, 1995*, Newport Beach, pp. 311–322.
- Haftka, R. T. and Z. Gurdal (1992). *Elements of Structural Optimization* (Third ed.). Norwell, MA: Kluwer.
- Hale, F. J. (1973). *Introduction to Control System Analysis and Design*. Prentice Hall.
- Haykin, S. (1996). *Adaptive Filter Theory* (Third ed.). Prentice Hall.
- Horta, L. G., J.-N. Juang, and C.-W. Chen (1993, October). Frequency domain identification toolbox. Technical Report TM-109039, NASA.
- Houston, B., M. Marcus, J. Bucaro, E. Williams, and D. Photiadis (1996, June). The structural acoustics and active control of interior noise in a ribbed cylindrical shell. *Journal of the Acoustical Society of America* 99(6), 3497–3512.
- Jolliffe, I. (1986). *Principal Component Analysis*. Springer-Verlag.
- Jones, J. D. and C. R. Fuller (1987, October). Active control of sound fields in elastic cylinders by multi-control forces. In *AIAA 11th Aeroacoustics Conference, Palo Alto, CA, October 19–21, 1987*, Number AIAA 87-2707. AIAA.
- Juang, J.-N. (1994). *Applied System Identification*. Prentice Hall.
- Kinsler, L. E., A. R. Frey, A. B. Coppens, and J. V. Sanders (1982). *Fundamentals of Acoustics* (Third ed.). John Wiley and Sons.
- Kuo, S. M. and D. R. Morgan (1996). *Active Noise Control Systems*. John Wiley and Sons.
- Lancaster, P. (1964). On eigenvalues of matrices dependent on a parameter. *Numerische Mathematik* 6, 377–387.
- Lee, J. C. and C. K. Un (1986, June). Performance of transform-domain lms adaptive digital filters. *IEEE Transactions on Acoustics, Speech, and Signal Processing* ASSP-34(3), 499–510.
- Leissa, A. W. (1973). Vibration of shells. Technical Report SP-288, NASA.
- Lester, H. and C. Fuller (1986, July). Active control of propeller induced noise fields inside flexible cylinder. In *AIAA 10th Aeroacoustics Conference, Seattle, WA, July 9–11, 1986*, Number AIAA 86-1957. AIAA.
- Lester, H. C. and S. Lefebvre (1993, July). Piezoelectric actuator models for active sound and vibration control of cylinders. *Journal of Intelligent Material Systems and Structures* 4, 295–306.
- Lester, H. C. and R. J. Silcox (1992, July). Active control of interior noise in a large scale cylinder using piezoelectric actuators. Technical Report 10103, NASA.
- Marshall, D. F. and W. K. Jenkins (1992, July). A fast quasi-newton adaptive filtering algorithm. *IEEE Transactions on Signal Processing* 40(7), 1652–1662.
- Marshall, D. F., W. K. Jenkins, and J. J. Murphy (1989, April). The use of orthogonal transforms for improving performance of adaptive filters. *IEEE Transactions on Circuits and Systems* 36(4), 474–483.

- Meirovitch, L. (1980). *Computational Methods in Structural Dynamics*. Sijthoff & Noordhoff.
- Meirovitch, L. (1990). *Dynamics and Control of Structures*. John Wiley and Sons.
- Miller, K. S. (1973, October). Complex linear least squares. *SIAM Review* 15(4), 706-726.
- Morgan, D. R. (1980). An analysis of multiple correlation cancellation loops with a filter in the auxiliary path. *IEEE Transactions on Acoustics, Speech, and Signal Processing ASSP-28*(4), 454-467.
- Morgan, D. R. (1991, January). An adaptive modal-based active control system. *Journal of the Acoustical Society of America* 89(1), 248-256.
- Nelson, P. A. and S. J. Elliott (1992). *Active Control of Sound*. Academic Press.
- Nelson, P. A., S. J. Elliott, A. J. Bullmore, and A. R. D. Curtis (1987). The active minimisation of harmonic enclosed sound fields; parts I, II, and III. *Journal of Sound and Vibration* 117, 1-58.
- Nelson, R. B. (1976, September). Simplified calculation of eigenvector derivatives. *AIAA Journal* 14(9), 1201-1205.
- Omoto, A. and S. Elliott (1997, August). The effect of structured plant uncertainty on the stability and performance of multichannel feedforward controllers. In *Active 97, Budapest Hungary, August 21-23, 1997*, pp. 825-836.
- Paillard, B., C. T. L. Donh, A. Berry, and J. Nicolas (1995). Accelerating the convergence of the filtered-x lms algorithm through transform-domain optimisation. *Mechanical Systems and Signal Processing* 9(4), 445-464.
- Palumbo, D. L., S. L. Padula, K. H. Lyle, J. H. Cline, and R. H. Cabell (1996, May). Performance of optimized actuator and sensor arrays in an active noise control system. In *2nd AIAA/CEAS Aeroacoustics Conference (17th Aeroacoustics Conference), State College, PA, May 6-8, 1996*, Number AIAA 96-1724.
- Panda, G., B. Mulgrew, C. F. Cowan, and P. M. Grant (1986, December). A self-orthogonalizing efficient block adaptive filter. *IEEE Transactions on Acoustics, Speech, and Signal Processing ASSP-34*(6), 1573-1582.
- Risi, J. and R. Burdisso (1994). Analytical investigation of adaptive control of radiated inlet noise from turbofan engines. In *Proceedings of Noise-Con 94, Ft. Lauderdale, Florida*, pp. 395-402.
- Rosenthal, F. (1992, March). A new technique for the active cancellation of wide-band noise using multiple sensors. In *Second International Congress on Recent Developments in Air- and Structure-Borne Sound and Vibration*, Auburn University, pp. 337-344.
- Ross, C. and M. Purver (1997, August). Active cabin noise control. In *Active 97, Budapest Hungary, August 21-23, 1997*, pp. 39-56.
- Rossetti, D. J., M. R. Jolly, and S. C. Southward (1996, May). Control effort weighting in feedforward adaptive control systems. *Journal of the Acoustical Society of America* 99(5), 2955-2964.
- Ruckman, C. and C. Fuller (1995). A regression approach for simulating feedforward active noise control. *Journal of the Acoustical Society of America* 97(5), 2906-2918.
- Ruckman, C. E. (1994, May). *A Regression-Based Approach for Simulating Active Noise Control in the Frequency Domain, with Application to Fluid-Structure Interaction Problems*. Ph. D. thesis, Virginia Polytechnic Institute and State University, Blacksburg, VA 24061.
- Ruckman, C. E. and C. R. Fuller (1993, April). Optimizing actuator locations in feedforward active control systems using subset selection. In *Second Conference on Recent Advances in Active Control of Sound and Vibration*, Blacksburg, Virginia, pp. S122-S133.
- S. Shankar Narayan, Allen M. Peterson, M. J. N. (1983). Transform domain lms algorithm. *IEEE Transactions on Acoustics, Speech, and Signal Processing ASSP-31*(3), 609-615.

- Silcox, R., C. Fuller, and H. Lester (1987, October). Mechanisms of active control in cylindrical fuselage structures. In *AIAA 11th Aeroacoustics Conference, Sunnyvale, CA, October 19-21, 1987*, Number AIAA 87-2703. AIAA.
- Silcox, R., H. Lester, and S. Abler (1989). An evaluation of active noise control in a cylindrical shell. *Journal of Vibration, Acoustics, Stress, and Reliability in Design* 111, 337-342.
- Snyder, S. and K. Burgemeister (1996). Performance enhancement of structural/acoustic active control systems via acoustic error signal decomposition. In *Inter-Noise 96; Proceedings of the International Congress on Noise Control Engineering*, pp. 1141-1146.
- Snyder, S. D. and C. H. Hansen (1991). Using multiple regression to optimize active noise control system design. *Journal of Sound and Vibration* 148(3), 537-542.
- Sommerfeldt, S. D., J. W. Parkins, and Y. C. Park (1995, July). Global active noise control in rectangular enclosures. In *Active 95, Newport Beach, CA, July 6-9, 1995*, Newport Beach, pp. 477-488.
- Sommerfeldt, S. D. and J. Tichy (1990, August). Adaptive control of a two-stage vibration isolation mount. *Journal of the Acoustical Society of America* 88(2), 938-944.
- Strang, G. (1988). *Linear Algebra and its Applications*. Harcourt Brace Jovanovich.
- Swanson, D. C. (1993, April). The generalized multichannel filtered-x algorithm. In *Second Conference on Recent Advances in Active Control of Sound and Vibration*, Blacksburg, Virginia, pp. 550-561.
- Thomas, D. R., P. A. Nelson, and S. J. Elliott (1993). Active control of the transmission of sound through a thin cylindrical shell, part II: The minimization of acoustic potential energy. *Journal of Sound and Vibration* 167(1), 113-128.
- Thomas, R. H., R. A. Burdisso, C. R. Fuller, and W. F. O'Brien (1994, January). Active control of fan noise from a turbofan engine. *AIAA Journal* 32(1), 23-30.
- Wallace, C. E. (1972). Radiation resistance of a rectangular panel. *Journal of the Acoustical Society of America* 51(3), 946-952.
- Walpole, R. E. and R. H. Myers (1985). *Probability and Statistics for Engineers and Scientists* (Third ed.). Macmillan.
- Watkins, D. S. (1991). *Fundamentals of Matrix Computations*. John Wiley and Sons.
- Widrow, B., J. R. G. Jr., J. M. McCool, J. Kaunitz, C. S. Williams, R. H. Hearn, J. R. Zeidler, E. D. Jr., and R. C. Goodlin (1975, December). Adaptive noise cancelling: Principles and applications. *Proceedings of the IEEE* 63(12), 1692-1716.
- Widrow, B. and J. M. E. Hoff (1960). Adaptive switching circuits. In *Proceedings IRE WESCON Convention Record, Part 4, Session 16*, pp. 96-104.
- Widrow, B. and S. D. Stearns (1985). *Adaptive Signal Processing*. Prentice-Hall.

# Vita

Randolph H. Cabell

Randolph Cabell was born in Melbourne, Florida on August 12, 1965 and was raised in Northern Virginia. He enrolled in Virginia Polytechnic Institute and State University in the fall of 1983 to study Mechanical Engineering. After graduating with a Bachelor's degree in 1987, he immediately started his Master's degree in Mechanical Engineering with Dr. Chris Fuller. The title of his Master's thesis was "The Automatic Identification of Aerospace Acoustic Sources," and described the application of adaptive techniques to learn to distinguish the sounds made by various transportation noise sources. Following his Master's degree, Mr. Cabell worked with Dr. Fuller as a Research Associate, in residence in the Applied Acoustics Branch at the NASA Langley Research Center in Hampton, Virginia. His topics of research included: neural networks for the automatic identification of helicopter noise; neural networks for fatigue damage prediction due to oscillating loads in the rotor system of helicopters; and neural networks for optimizing actuator groupings for the feedforward control of aircraft interior noise. This last research topic provided the motivation for the topic of his dissertation. In April of 1998, he received his PhD in Mechanical Engineering, and accepted a National Research Council Associateship Award in the Structural Acoustics Branch at NASA Langley Research Center.